ISSN 1063-780X, Plasma Physics Reports, 2009, Vol. 35, No. 5, pp. 399–408. © Pleiades Publishing, Ltd., 2009.
Original Russian Text © A.A. Solov'ev, N.S. Sochugov, K.V. Oskomov, S.V. Rabotkin, 2009, published in Fizika Plazmy, 2009, Vol. 35, No. 5, pp. 443–452.

PLASMA DIAGNOSTICS

Investigation of Plasma Characteristics in an Unbalanced Magnetron Sputtering System

A. A. Solov'ev, N. S. Sochugov, K. V. Oskomov, and S. V. Rabotkin

Institute of High Current Electronics, Siberian Branch, Russian Academy of Sciences, Tomsk, 634055 Russia

Received July 1, 2008; in final form, November 12, 2008

Abstract—Results are presented from experimental studies of a magnetron sputtering system for different configurations of the magnetic field above the cathode surface. The current–voltage characteristics of a magnetron discharge at different working gas pressures (0.08–0.3 Pa) and currents in the unbalancing coil were studied. The production and transport of charge carriers in a magnetron discharge with an unbalanced magnetic field was investigated by means of probe measurements of plasma characteristics and ion energies in the region between the substrate and the magnetic trap at the cathode surface. The radial distributions of the ion current density, plasma potential, and floating potential in the unbalanced operating mode are found to have pronounced extrema at the magnetron axis. It is shown that the plasma density near the substrate can be increased considerably when the axial magnetic field is high enough to efficiently confine plasma electrons and prevent their escape to the chamber wall.

PACS numbers: 52.50.Dg, 52.70.Ds, 52.77.Dq

DOI: 10.1134/S1063780X09050055

1. INTRODUCTION

Magnetron sputtering systems are widely used in electronics, optical industry, and mechanical engineering to deposit thin films. These systems are based on the excitation of a volume electric discharge in a rarefied gaseous medium in which there are regions with crossed electric and magnetic fields. The possibility of controlling the plasma parameters over a wide range in the course of deposition is an important property of magnetron sputtering systems. The requirements for the controlled plasma parameters depend on a particular problem and the designation of the coating. It is well known that the structure and properties of a coating can be changed by varying the ion current density J_i to the substrate in the range of about 0.2–2 mA/cm^2 and the energy E_i of bombarding ions from several electronvolts to a few hundred electronvolts [1]. The ion energy can easily be controlled by applying a negative voltage to the conducting substrate; however, the ion current is limited by the plasma density near the substrate. In conventional magnetron sputtering systems, this density drops exponentially with increasing distance from the cathode. The problem of generating the required ion current density can be solved by using magnetrons equipped with electromagnetic coils that allow one to flexibly control the strength and configuration of the magnetic field [2, 3]. However, at present, such magnetrons have not yet received widespread use because they are rather difficult to manufacture and the effect of the magnetic configuration on the operating parameters of a magnetron discharge is still poorly understood. Unfortunately, information on the spatial distribution of the plasma parameters (especially in magnetrons with an unbalanced magnetic field) is very scarce. Although magnetron plasmas have been studied using electric probes [4–7] and optical spectroscopy [8, 9], these studies were performed in limited spatial regions and are insufficient to construct a complete picture of the spatial distributions of the plasma parameters.

The objective of this work was to experimentally determine the distributions of the plasma parameters in the region between the cathode and the substrate in a magnetron sputtering system with an electromagnetic coil that allows one to widely vary the configuration of the magnetic field above the cathode surface. The main goal of this work was to study how the distributions of the plasma parameters depend on the distribution of the magnetic field.

The objective of this work was to experimentally determine the distributions of the plasma parameters in the region between the cathode and the substrate in a magnetron sputtering system with an electromagnetic coil that allows one to widely vary the configuration of the magnetic field above the cathode surface. The main goal of this work was to study how the distributions of the plasma parameters depend on the distribution of the magnetic field.

2. EXPERIMENTAL SETUP

A schematic of the magnetron sputtering system with an electromagnetic coil is shown in Fig. 1. The experiments were performed in a 600 × 600 × 600-mm

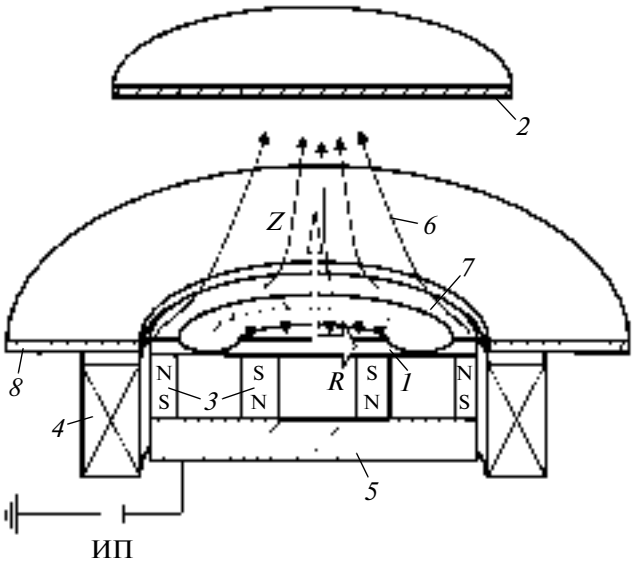

Fig. 1. Simplified schematic of the magnetron sputtering system: (*1*) cathode, (*2*) substrate, (*3*) permanent magnets, (*4*) solenoid, (*5*) magnetic circuit, (*6*) unbalanced magnetic field lines, (*7*) balanced magnetic field lines, (*8*) anode, and (*PS*) magnetron power supply.

stainless-steel vacuum chamber. The magnetron was attached to the vacuum chamber via a mounting flange, which, as well as the wall of the vacuum chamber, served as an anode of the magnetron discharge. The magnetron cathode was a 95-mm-diameter 6-mm-thick titanium disk cooled with water. The axisymmetric magnetic system consisted of a central and a peripheral ring permanent (NdFeB) magnet, a magnetic conductor, and a coaxial electromagnetic coil with 3500 turns of a copper wire with a current of up to 1 A.

The distribution of the magnetic field above the cathode was calculated using the ELCUT code intended for engineering simulations of electromagnetic, thermal, and other problems by using the well-known finite-element method. The magnetic field produced by the magnetic system on the cathode surface and the magnetron axis in the magnetron–substrate space was also measured with an RSh 1-10 magnetometer.

The main parameters measured in our experiments were the argon pressure, the discharge power, and the current in the electromagnetic coil. The pressure in the vacuum chamber was controlled by varying the flow rate of the working gas supplied to the chamber. The working gas pressure was varied from 0.8×10^{-1} to 3×10^{-1} Pa; the discharge power, from 0.5 to 2 kW; and the current in the electromagnetic coil, from 0 to 1 A.

The ion current to the substrate was measured using a 330-cm^2 collector, which was installed at a distance of 23 cm from the magnetron and to which a pulsed negative voltage with an amplitude of 100 V, a frequency of 18 kHz, and a period-to-pulse ratio of 50% was supplied.

The ion current density J_i to the substrate and the floating potential $V_{\rm fl}$ were determined using a plane probe with a guard ring. The guard ring surrounding the 11.8-mm-diameter stainless-steel central electrode of the probe was at the same potential as the central electrode and served to minimize edge effects [10]. The probe was placed at the substrate in such a way that its working surface was in the substrate plane.

The plasma potential $V_{\rm pl}$ was determined by measuring the floating potential of an emissive probe (see [11]). As the filament current is increased, the probe is heated and the probe emission current increases, which leads to an increase in the probe floating potential. When the emission current becomes equal to the electron current from the plasma to the probe, the floating potential of the probe becomes equal to the plasma potential. Using probes, we measured the radial distributions of the above plasma parameters at different distances from the cathode.

To better understand the effect of ion bombardment during magnetron deposition, it is necessary to have more information on the energy distributions of ions bombarding the surface under different deposition conditions. Therefore, we performed measurements of the energy spectra of positive ions in a magnetron discharge by using a HIDEN EQP 45° electrostatic analyzer. The analyzer was placed on the magnetron axis at a distance of 13.5 cm from its cathode. The diameter of the aperture through which the ions were extracted from discharge plasma was 0.1 mm.

To better understand the effect of ion bombardment during magnetron deposition, it is necessary to have more information on the energy distributions of ions bombarding the surface under different deposition conditions. Therefore, we performed measurements of the energy spectra of positive ions in a magnetron discharge by using a HIDEN EQP 45° electrostatic analyzer. The analyzer was placed on the magnetron axis at a distance of 13.5 cm from its cathode. The diameter of the aperture through which the ions were extracted from discharge plasma was 0.1 mm.

3. RESULTS AND DISCUSSION

The calculated distributions of the magnetic field above the cathode surface are shown in Fig. 2. Since the numerical model is symmetric with respect to the Z axis (Fig. 1), Fig. 2 shows only the left halves of the distributions. It is seen that, depending on the value and direction of the current $I_{\tilde{n}}$ in the electromagnetic coil, either a balanced or an unbalanced (type 1 or 2, according to the accepted terminology [12]) magnetic configuration can form above the cathode surface. The

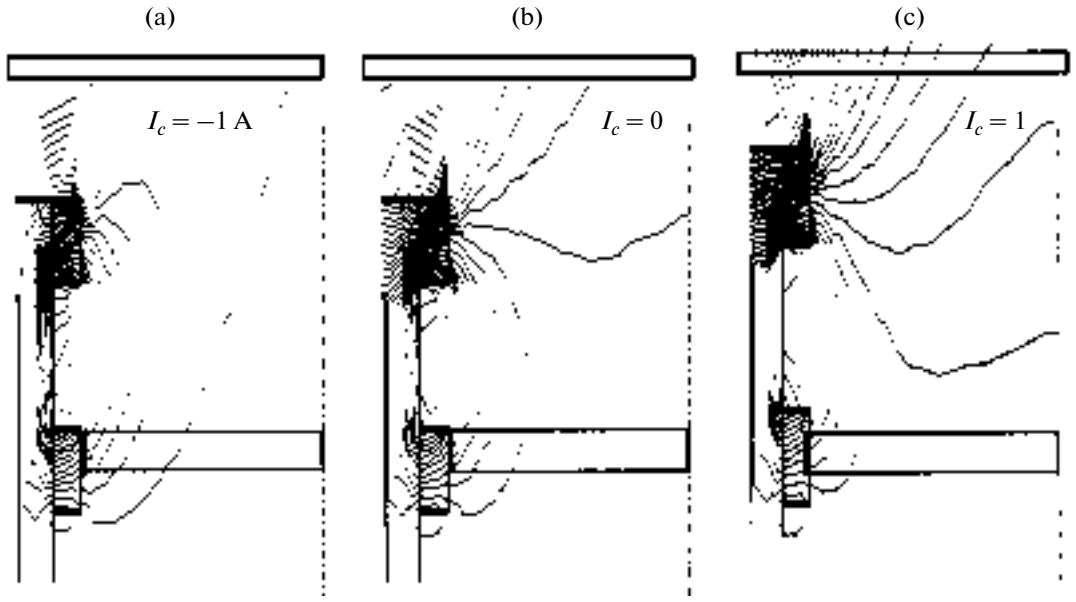

Fig. 2. Configuration of the magnetic field above the cathode surface for different values and directions of the current I_c in the electromagnetic coil: (a) unbalanced magnetron (type 1), (b) weakly unbalanced magnetron (type 2), and (c) highly unbalanced magnetron (type 2).

type-1 unbalanced magnetic configuration has not received widespread use, because, in this configuration, the unbalanced field lines are directed toward the chamber wall; as a result, the plasma density near the substrate is low. Therefore, the type-2 unbalanced magnetic configuration is more suitable for the generation of ions near the substrate. This configuration forms when the direction of the solenoid magnetic field coincides with that of the magnetic field produced by the external magnets of the magnetron (I_c = 1 A).

To estimate the degree to which the magnetic field was unbalanced, we used the coefficient of the geometric unbalance K_G, which was calculated by the formula

$$K_G = Z_0/2R$$

where Z_0 is the distance to the null point (a point on the magnetron axis at which the magnetic field changes its direction) and R is the average radius of the erosion zone [13].

For the given magnetron design, K_G can vary within the interval 0.3–3.3, depending on the current in the electromagnetic coil.

In addition to magnetic field calculations, we also performed direct measurements of the magnetic field at different values of the current in the electromagnetic coil. The results of these measurements are presented in Fig. 3. The tangential component of the magnetic field above the cathode surface is minimum (550 G) at $I_c = 1$ A. The radius of the sputtering region is also minimum at this current value. This is because, in a highly unbalanced regime (type 2), the magnetic trap above the cathode surface is pressed by the force lines of the unbalanced magnetic field toward the center of the cathode. The inhomogeneity of the magnetic field above the cathode surface (Fig. 3a) leads to plasma localization in the region where the magnetic field is maximum and the formation of a narrow erosion groove. Due to the arch shape of the magnetic field, the use factor of the cathode is usually 25–30%. To enlarge the cathode sputtered area and, hence, increase the use factor of the cathode, systems in which magnets are displaced along the surface of a plane cathode or cylindrical cathodes are rotated about stationary magnetic systems are often used. However, these methods considerably complicate the magnetron design. Therefore, in some cases, it is simpler to move the sputtering region along the cathode surface (rather than mechanically displacing the magnets or the cathode) by supplying the electromagnetic coil with an ac current. In this case, the range within which the radius of the sputtering region varies with the frequency of the ac solenoid current depends on the configuration of the magnetic field.

In the type-1 unbalanced regime (I_c = –1 A), the normal component the magnetic field component on the system axis decreases exponentially to zero (Fig. 3b). When the electromagnetic coil is switched off, the magnetron operates in the type-2 weakly unbalanced regime. As the solenoid current increases to 1 A, the magnetic field lines become more unbalanced and the maximum value of the magnetic field on the magnetron axis reaches 180 G.

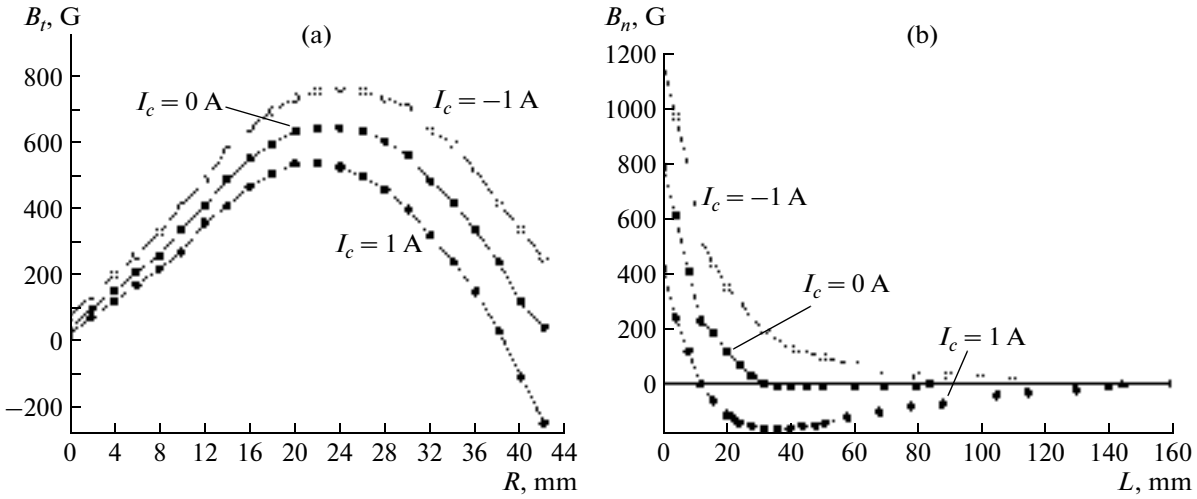

Fig. 3. (a) Radial distributions of the tangential magnetic field component above the cathode surface and (b) axial distributions of the normal magnetic field component at the magnetron axis for different values of the current in the electromagnetic coil.

One of the most important characteristics of a magnetron discharge is its current–voltage characteristic, which depends substantially on the working pressure P and the magnetic induction B. The current of the magnetron discharge is determined by many factors, such as the source power, the discharge voltage, the sort and pressure of the working gas, the magnetic induction, the configuration of the magnetron system, and the sputtered material.

Figure 4 shows the current–voltage characteristic of a magnetron discharge at different argon pressures in the vacuum chamber. At discharge currents from 0.1 to 5 A, the operating voltage varies from 300 to 520 V.

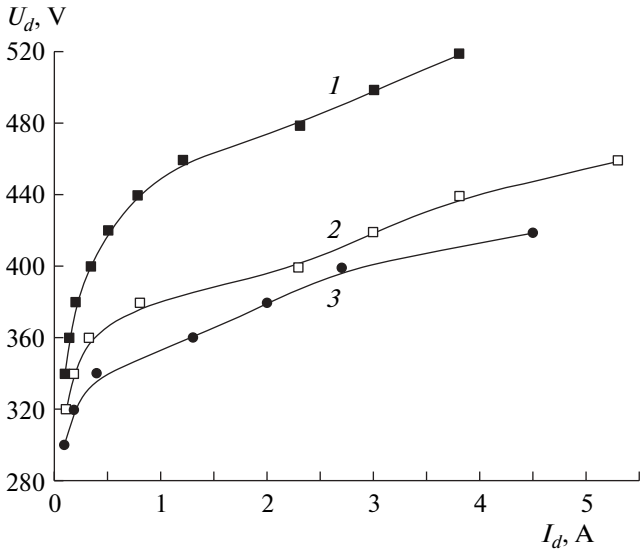

Fig. 4. Current–voltage characteristics of the discharge at different working gas pressures (the electromagnetic coil switched off): P_{Ar} = (*1*) 0.08, (*2*) 0.2, and (*3*) 0.3 Pa.

As the gas pressure decreases, the current–voltage characteristic shifts toward higher operating voltages. When the electromagnetic coil is switched on, the discharge voltage increases and the current–voltage characteristic shifts toward higher operating voltages, as is in the case in which the pressure is decreased (Fig. 5). This is because, in the unbalanced regime, the shape of the magnetic trap near the cathode surface is distorted. As the current in the electromagnetic coil increases, the magnetic field in the trap near the cathode decreases (Fig. 3a), while the discharge voltage increases. As a result, the energy of electrons leaving the trap becomes greater.

When the collector is biased negatively, it extracts ions. The voltage at which the ion current becomes saturated is about 60 V. As the magnetron discharge current increases from 1 to 4 A, the ion current to the collector increases from 80 to 250 mA. When the electromagnetic coil is switched on, the ion current extracted to the collector increases considerably (Fig. 6). This is mainly related to the lengthening of the trajectories of ionizing electrons in the axial magnetic field.

Figure 7 shows the results of measurement of the density of the ion saturation current to the probe at the distance L = 150 mm from the cathode for different currents in the electromagnetic coil. The discharge power was maintained at a constant level of 0.6 W. The increase in the current in the electromagnetic coil is accompanied by a considerable increase in the ion current density. This effect, which is most pronounced on the system axis, is explained by the increase in the imbalance of the magnetic field, the force lines of which are directed toward the substrate, thereby limiting the transverse electron mobility and causing electrons to move along the system axis. In this case, electrons move together with ions, because the plasma

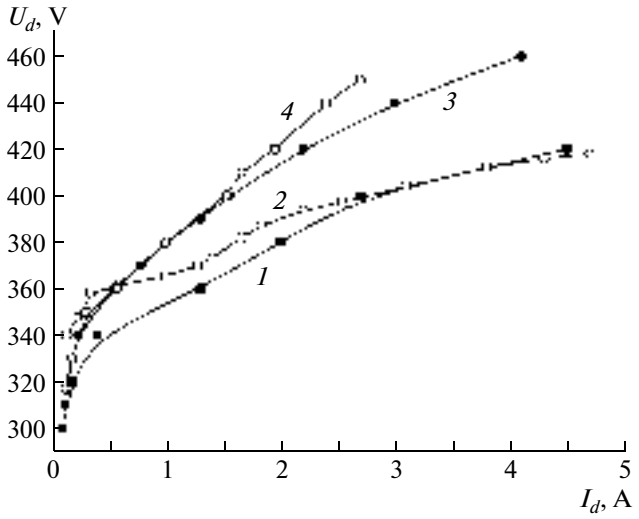

Fig. 5. Current–voltage characteristics of the discharge at $P_{Ar} = 0.08$ Pa and different currents in the electromagnetic coil: $I_c = (1)$ 0, (2) 0.3, (3) 0.6, and (4) 0.9 A.

should be kept electrically neutral [14]. Visually, the increase in the solenoid current is accompanied by a decrease in the radius of the glowing region on the cathode and the appearance of a plasma flow directed toward the substrate on the system axis (Fig. 8).

Measurements of the floating potential and the plasma potential in the maximally unbalanced regime ($I_c = 1$ A) at different distances from the cathode show that the spatial distributions of these parameters are very nonuniform (see Figs. 9, 10). As the distance from the cathode increases, the radial distributions of V_{fl} and V_{pl} become flatter and have no pronounced extrema on the system axis.

The lowest floating potential (down to −25 V) was observed near the cathode and on the system axis. As the distance from the cathode and the system axis increased, the absolute value of the floating potential decreased to several units of volts. The floating potential is known to be determined by the ion and electron fluxes to the probe, which in turn depend on the density and energy of ions and electrons. Since the plasma is assumed to be quasineutral and the electron mobility is considerably higher than the ion mobility, the floating potential mainly depends on the electron energy [15]. Thus, in [15], this was confirmed by measurements of the spatial distributions of the floating potential and electron temperature by a cylindrical Langmuir probe. Regions with a high electron temperature were found to correspond to those with a high floating potential. The electron temperature in a balanced magnetron was shown to be maximum near the magnetic trap at the cathode surface and decrease with distance from the cathode. Therefore, it can be assumed that, in our case, the electron temperature is maximum near the cathode and on the magnetron axis and decreases in the region where the magnetic field is weak.

Applying the additional magnetic field leads to (i) a decrease in the plasma potential near the cathode and on the system axis due to the magnetic confinement of electrons and (ii) the formation of a radial potential well for ions, which prevents them from leaving the well in the radial direction. The plasma potential in a magnetron discharge with an unbalanced magnetic

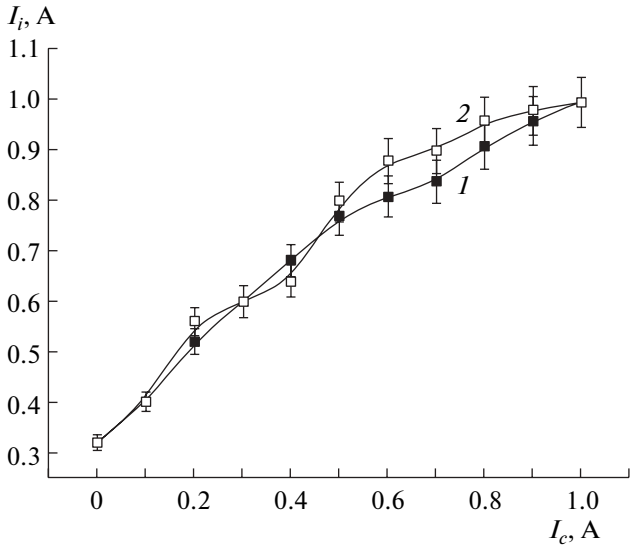

Fig. 6. Ion current to the collector I_i as a function of current I_c in the electromagnetic coil for $P_{Ar} = 0.3$ Pa, $U_{bias} = -100$ V, a discharge power of 2 kW, and different repetition frequencies of the bias voltage: $f = (1)$ 18 and (2) 100 kHz.

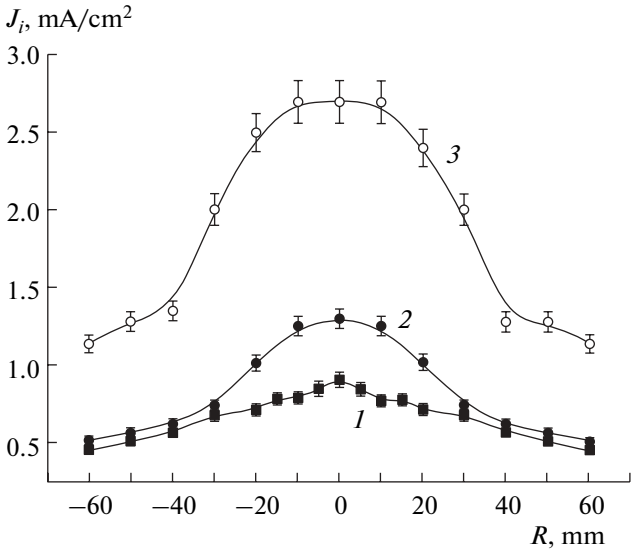

Fig. 7. Radial distributions of the ion current density at a distance of 150 mm from the cathode for a discharge power 0.6 kW and different solenoid currents: $I_c = (1)$ 0, (2) 0.5, and (3) 1 A.

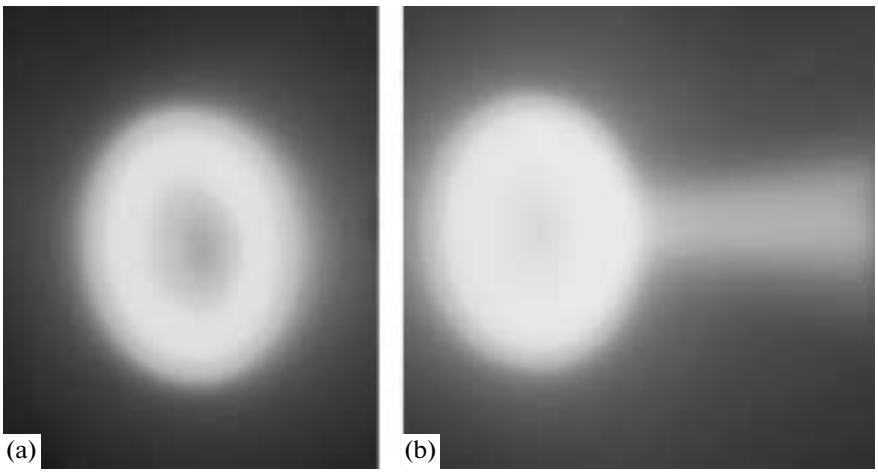

Fig. 8. Plasma glow at the cathode (a) for the case in which the electromagnetic coil is switched off and (b) for the maximum current (1 A) in the electromagnetic coil.

field is negative because the plasma is confined by the magnetic field between the negatively biased cathode and the substrate [16].

The electrons that leave the magnetic trap near the cathode surface move then toward the anode, thereby balancing the ion flux to the cathode and maintaining stable operation of the discharge. As a rule, electron transport in plasma is described using the classical diffusion model, which assumes the presence of a nonzero gradient of the plasma potential that maintains balance between electron and ion fluxes. According to this model, the electron flux along the magnetic field is

$$\Gamma_{ez} = -\mu_e n_e E_z - D_e \frac{\partial n_e}{\partial z},$$

where μ_e is the electron mobility, D_e is the electron diffusion coefficient, E_z is the axial electric field ($E_z = -\partial V_p/\partial z$), and V_p is the plasma potential.

The literature data on the spatial distributions of the plasma potential in a magnetron discharge are rather contradictory. In some experiments, large axial variations ΔV_p in the plasma potential between the cathode sheath and the substrate were observed. Thus, in [17], axial variations in the plasma potential were

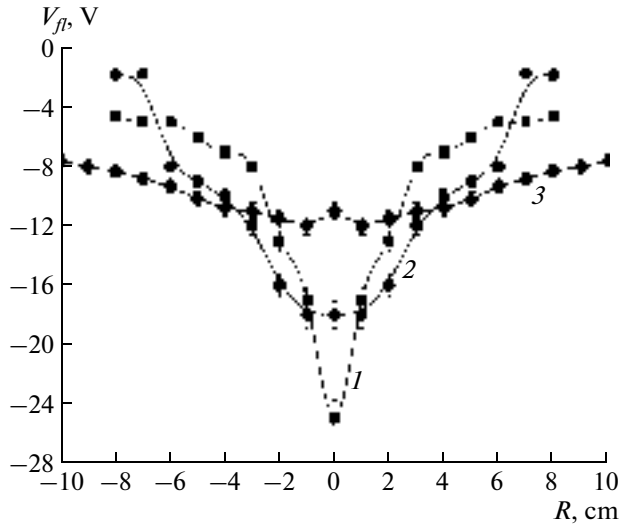

Fig. 9. Radial distributions of the floating potential for at different distances L from the cathode for $P_{Ar} = 0.2$ Pa, $I_c = 1$ A, and a discharge power of 0.5 kW: $L = (1)$ 6, (2) 10, and (3) 22 cm.

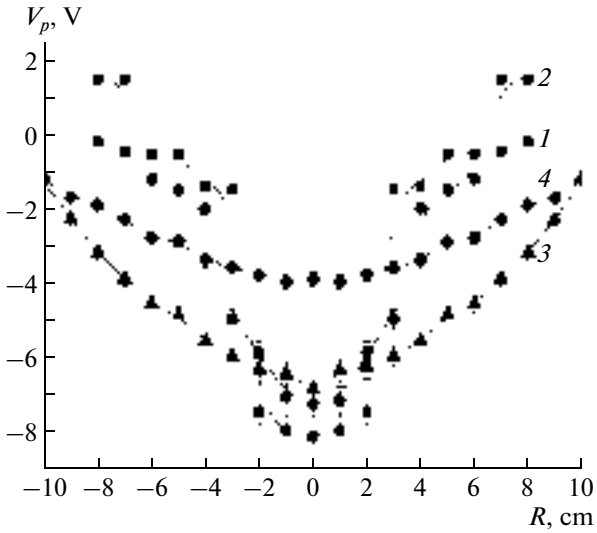

Fig. 10. Radial distributions of the plasma potential at different distances L from the cathode for $P_{Ar} = 0.2$ Pa, $I_c = 1$ A, and a discharge power of 0.5 kW: $L = (1)$ 6, (2) 10, (3) 15, and (4) 22 cm.

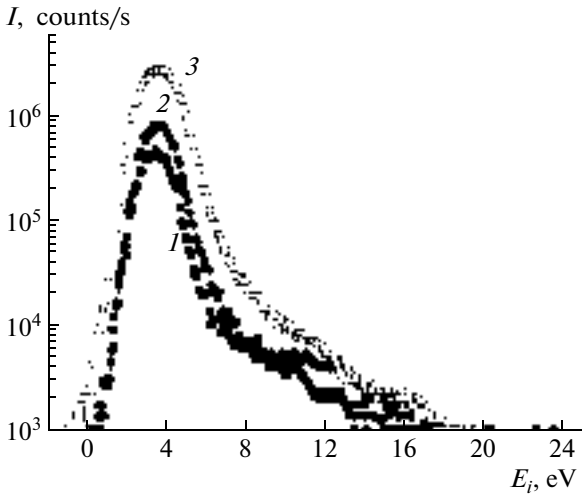

Fig. 11. Energy spectra of argon ions for $P_{Ar} = 0.15$ Pa, $I_c = 0$ A, and different discharge powers: $P = (1)$ 0.5, (2) 1, and (3) 1.5 kW.

found to be as large as $\Delta V_p \sim 20$ V, while in [18], they were up to ~40 V. On the other hand, in [19], comparatively flat axial potential distributions with ΔV_p of a few volts were observed.

Along with the gradients of the electric potential and electron density, there is another factor causing electrons to move toward the substrate—the axially diverging magnetic field. In such a field, electrons are affected by the force described by the expression [20]

$$F_z = -\frac{m_e v_n^2}{2B_z}\frac{\partial B_z}{\partial z},$$

where v_n is the electron velocity component perpendicular to the magnetic field.

The force F_z expels electrons toward the region with a weaker field. However, in this case, electrons gain no energy, because the magnetic field does not perform any work.

In our case, as is seen in Fig. 10, the plasma potential rises with decreasing distance from the anode. As the distance from the cathode increases from 6 to 22 cm, the plasma potential increases by $\Delta V_p \sim 4$ V. When an external magnetic field is applied to the system, the plasma potential decreases on the whole due to a decrease in the electron Larmor radius and, accordingly, more efficient confinement of plasma electrons. When the magnetic field is sufficiently strong, electrons can move across the magnetic field lines over a distance larger than the Larmor radius only due to multiple elastic collisions. Therefore, in order to efficiently confine electrons and prevent them from escaping to the chamber wall, the electron Larmor radius should be much smaller than the characteristic dimensions of the chamber. In this case, electrons are "attached" to magnetic field lines, while the ion motion is determined by the electric field produced by charge separation in plasma.

Thus, the number of ions near the substrate in a magnetron discharge with an unbalanced magnetic field is relatively large because it is necessary to maintain plasma quasineutrality under the conditions of anode-directed electron motion caused by the gradients of the electric potential and electron density, as well as by the axial divergence of the magnetic field.

When the substrate is biased negatively, the region where the electrons that left the magnetic trap near the

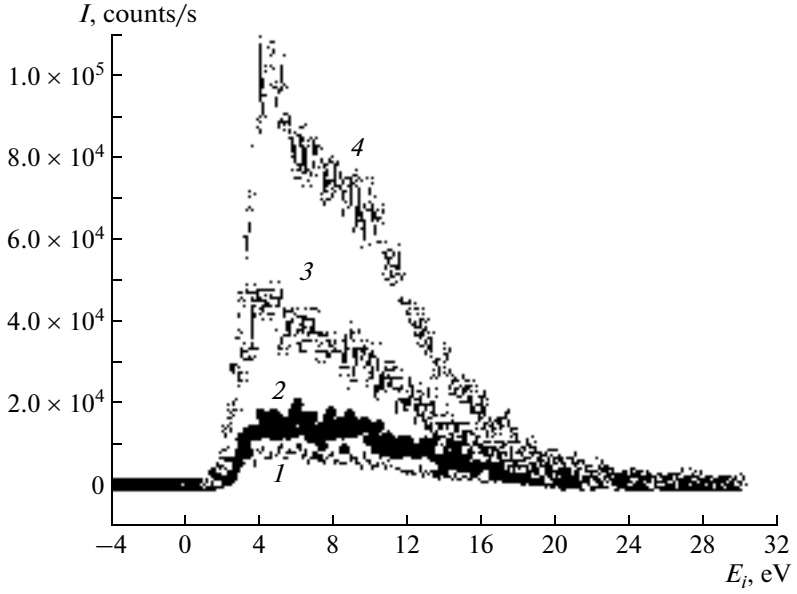

Fig. 12. Energy spectra of titanium ions for $P_{Ar} = 0.15$ Pa, $I_c = 0$ A, and different discharge powers: $P = (1)$ 0.5, (2) 1, (3) 1.5, and (4) 2 kW.

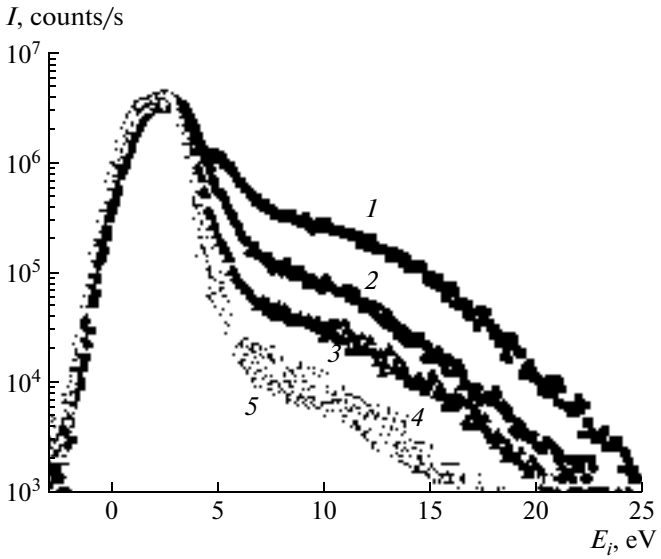

Fig. 13. Energy spectra of argon ions for $I_c = 0$ A, a discharge power of 0.5 kW, and different gas pressures: P_{Ar} = (*1*) 0.08, (*2*) 0.14, (*3*) 2, (*4*) 2.6, and (*5*) 3.2 Pa.

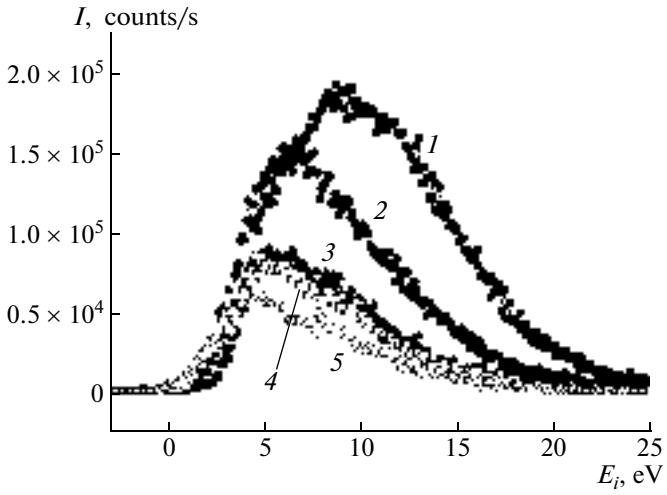

Fig. 14. Energy spectra of titanium ions for $I_c = 0$ A, a discharge power of 0.5 kW, and different gas pressures: P_{Ar} = (*1*) 0.08, (*2*) 0.14, (*3*) 2, (*4*) 2.6, and (*5*) 3.2 Pa.

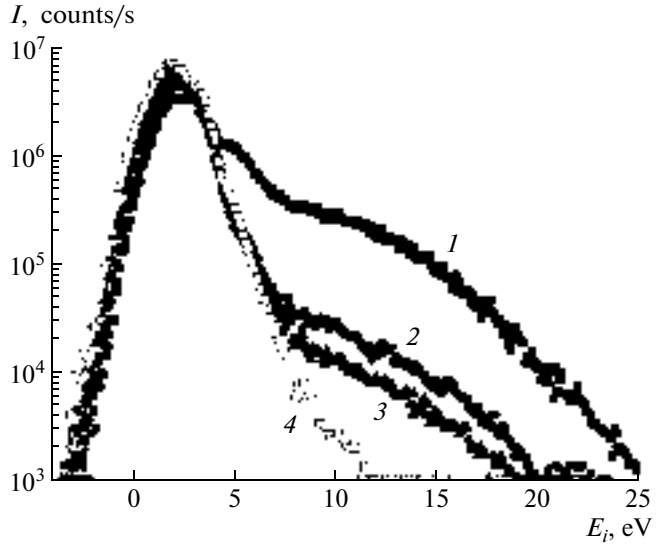

Fig. 15. Energy spectra of argon ions for $P_{Ar} = 0.08$ Pa, a discharge power of 0.5 kW, and different currents in the electromagnetic coil: I_c = (*1*) 0, (*2*) 0.2, (*3*) 0.4, and (*4*) 0.6 A.

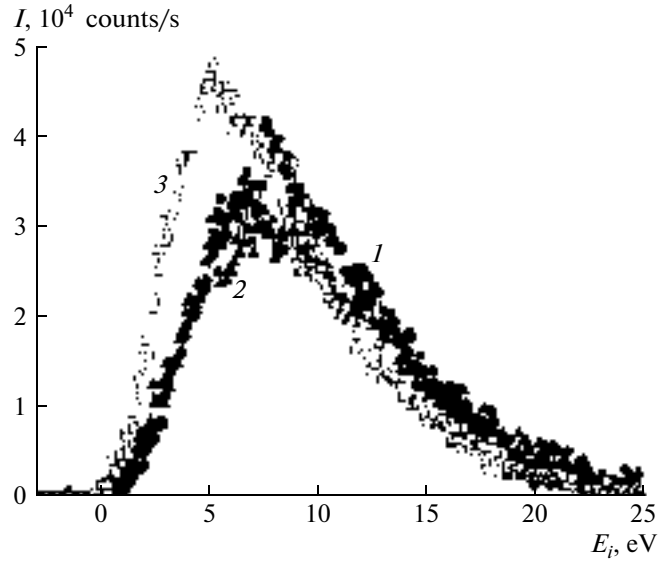

Fig. 16. Energy spectra of titanium ions for $P_{Ar} = 0.08$ Pa, a discharge power of 0.5 kW, and different currents in the electromagnetic coil: I_c = (*1*) 0.2, (*2*) 0.4, and (*3*) 0.6 A

cathode are situated is limited from one side by a relatively high negative potential of the substrate and, from the other sides, by regions with a relatively strong magnetic field. As a result, electrons oscillate along the magnetic field lines, due to which their energy is utilized more efficiently.

Figures 11–16 show the energy distributions of argon and titanium ions for different magnetron discharge powers (0.5–2 kW), argon pressures (0.08–0.32 Pa), and currents in the electromagnetic coil (0.2–0.6 A).

The energy spectra of argon and titanium ions have maxima at energies of about 3.5 and 5 eV, respectively, and high-energy tails in the energy range 5–30 eV (Figs. 11, 12). The maxima of the energy distributions correspond to thermalized ions, the energy of which is

determined by the difference between the plasma and anode potentials. In a magnetron discharge, this difference is usually a few volts [21]. It is seen from the energy spectra that most ions have corresponding energies. The appearance of high-energy tails cannot be attributed to the high plasma potential, because, in a magnetron discharge, such potentials are not observed [3]. There is a high negative potential (usually from −300 to −500 V) near the surface of the sputtered target, but this potential accelerates positive ions only toward the cathode. The presence of ions with energies of up to 20–30 eV can be explained by either reflection of neutralized ions from the cathode [3] or gas atoms acquiring energy in collisions with sputtered cathode atoms. In both cases, high-energy neutral atoms are then ionized in the plasma between the substrate and the magnetic trap near the cathode surface.

It can be seen from the intensities of the peaks that the number of titanium ions is only 1–2% of that of argon ions. Thus, the degree of ionization of metal atoms sputtered from the cathode is low. The intensities of the peaks increase with increasing discharge power, which is related to the increase in the plasma density in the measurement region (Figs. 11, 12).

In the energy spectra, there is always present a low-energy peak of thermalized Ar ions, the intensity and position of which are independent of the gas pressure in the chamber (Fig. 13). However, the intensity of the peak of Ar ions doubles as the current in the electromagnetic coil increases from 0 to 0.6 A (Fig. 15). The high-energy tail of Ar ions decreases considerably with increasing gas pressure and current in the electromagnetic coil. The decrease in the number of high-energy ions with increasing pressure is explained by an increase in the frequency of collisions of Ar ions with neutral atoms.

The intensity and position of the Ti ion peak depends substantially on the Ar pressure in the chamber (Fig. 14). As the pressure increases from 0.08 to 3.2 Pa, the intensity of this peak decreases fourfold and the maximum of the distribution shifts from 8 to 5 eV. The current in the electromagnetic coil insignificantly affects the energy spectra of Ti ions (Fig. 16); however, the energy of these ions can be controlled by varying the voltage applied to the processed articles.

The intensity and position of the Ti ion peak depends substantially on the Ar pressure in the chamber (Fig. 14). As the pressure increases from 0.08 to 3.2 Pa, the intensity of this peak decreases fourfold and the maximum of the distribution shifts from 8 to 5 eV. The current in the electromagnetic coil insignificantly affects the energy spectra of Ti ions (Fig. 16); however, the energy of these ions can be controlled by varying the voltage applied to the processed articles.

4. CONCLUSIONS

In our experiments, we have measured the spatial distributions of the plasma parameters in a magnetron sputtering system with an electromagnetic coil that allows obtaining various magnetic configurations. It is shown that, in order to increase the plasma density near the substrate, it is necessary to create an axial magnetic field between the substrate and the magnetron. The induction of this field must be high enough to efficiently confine plasma electrons and prevent them from drifting toward the chamber wall. In this case, the plasma parameters are distributed nonuniformly in the space between the magnetron and the substrate and the plasma potential can become negative. The ion current density and the floating potential are the largest on the magnetron axis and decrease with increasing distance from the magnetron and the system axis.

The energy distributions of ions in a magnetron discharge are nonequilibrium. They have maxima corresponding to thermalized particles that were ionized at the plasma potential and high-energy tails with energies of up to 20–30 eV. The intensity of the high-energy tail depends on the gas pressure in the chamber and the degree to which the magnetron is unbalanced. The main process affecting the ion energy distribution is collisional energy transfer from sputtered particles to gas atoms.

The energy distributions of ions in a magnetron discharge are nonequilibrium. They have maxima corresponding to thermalized particles that were ionized at the plasma potential and high-energy tails with energies of up to 20–30 eV. The intensity of the high-energy tail depends on the gas pressure in the chamber and the degree to which the magnetron is unbalanced. The main process affecting the ion energy distribution is collisional energy transfer from sputtered particles to gas atoms.

ACKNOWLEDGMENTS

This work was supported by the Russian Federal Agency on Science and Innovations, project no. GK 02.516.11.6117.

This work was supported by the Russian Federal Agency on Science and Innovations, project no. GK 02.516.11.6117.

REFERENCES

1. X. B. Zhang, J. Q. Xiao, Z. L. Pei, et al., J. Vac. Sci. Technol. A **25,** 209 (2007).
2. I. Petrov, F. Abibi, J. E. Greene, et al., J. Vac. Sci. Technol. A **10**, 3283 (1992).
3. I. Ivanov, P. Kazansky, L. Hultman, et al., J. Vac. Sci. Technol. A **12**, 314 (1994).
4. S. M. Rossnagel and H. R. Kaufman, J. Vac. Sci. Technol. A **4**, 1822 (1986).
5. T. E. Sheridan and J. Goree, J. Vac. Sci. Technol. A **7**, 1014 (1989).
6. I. Petrov, I. Ivanov, V. Orlinov, and J. Kourtev, Contrib. Plasma Phys. **30**, 223 (1990).

7. P. Spatenka, J. Vlcek, and J. Blazek, Vacuum **55**, 165 (1999).
8. L. Gu and M. A. Lieberman, J. Vac. Sci. Technol. A **6**, 2960 (1988).
9. S. Miyake, N. Shimura, T. Makabe, and A. Itoh, J. Vac. Sci. Technol. A **10**, 1135 (1992).
10. C. Engström, T. Berlind, J. Birch, et al., Vacuum **56**, 107 (2000).
11. I. Pickova, A. Marek, M. Tichy, and P. Kudrna, Czech. J. Phys. **56**, 1002 (2006).
12. B. Window and N. Savvides, J. Vac. Sci. Technol. A **4**, 453 (1986).
13. www.gencoa.com.
14. B. Window, G. L. Harding, J. Vac. Sci. Technol. A **8**, 1277 (1990).
15. D. J. Field, S. K. Dew, and R. E. Burrell, J. Vac. Sci. Technol. A **20**, 2032 (2002).
16. S. Kadlec, C. Quaeyhaegens, G. Knuyt, and L. M. Stals, Surf. Coat. Technol. **89**, 177 (1997).
17. H. Bingsen and C. Zhou, Surf. Coat. Technol. **50**, 111 (1992).
18. J. W. Bradley, R. D. Arnell, and D. G. Armour, Surf. Coat. Technol. **97**, 538 (1997).
19. S.-H. Seo, J.-H. In, and H.-Y. Chang, Plasma Sources Sci. Technol. **13**, 409 (2004).
20. M. A. Lieberman and A. J. Lichtenberg, *Principles of Plasma Discharges and Materials Processing* (Wiley, New York, 1994), p. 373.
21. M. Misina, L. R. Shaginyan, M. Macek, and P. Panjan, Surf. Coat. Technol. **142–144**, 348 (2001).
21. M. Misina, L. R. Shaginyan, M. Macek, and P. Panjan, Surf. Coat. Technol. **142–144**, 348 (2001).

Translated by E.G. Baldina

SPELL: OK